Fine-structure measurements in high-L $n=17$ and 20 Rydberg states of barium

E. L. Snow
Department of Physics, SUNY Fredonia, Fredonia, New York 14063, USA

S. R. Lundeen
Department of Physics, Colorado State University, Fort Collins, Colorado 80523, USA

(Received 31 August 2007; published 12 November 2007)

Fine-structure intervals in $n=17$ and 20 barium Rydberg levels with $6 \leq L \leq 11$ have been measured precisely with the resonant excitation Stark ionization spectroscopy microwave technique. The measured intervals were analyzed using the long-range polarization model, including allowance for the large nonadiabatic effects of the Ba^+ $5d$ level and the contributions of higher-order terms. The analysis determined improved values in atomic units of both dipole and quadrupole polarizabilities of Ba^+, $\alpha_1=123.88(5)$ and $\alpha_2=4420(250)$.

DOI: 10.1103/PhysRevA.76.052505 PACS number(s): 32.10.Dk, 32.10.Fn

I. INTRODUCTION

Studies of fine-structure patterns in nonpenetrating high-L Rydberg states can lead to determination of the core ion properties, such as polarizabilities and permanent moments. To achieve this, measurements need to encompass a sufficiently wide range of L's in states where core penetration is negligible, typically $L>5$. The resonant excitation Stark ionization spectroscopy (RESIS) method provides a convenient way to access the high-L levels needed for such studies, and has been used in the past to explore fine-structure patterns in several atoms, molecules, and ions [1]. In this work, the RESIS microwave method is used to explore the fine-structure patterns in $n=17$ and 20, $6 \leq L \leq 11$, Rydberg states of barium, leading to a determination of the dipole and quadrupole polarizabilities of the Ba^+ ion.

Studies of the barium ion are of particular interest because it is currently being used for studies of parity-violating weak interactions [2]. The connection between such measurements and fundamental interaction strengths depends on precise knowledge of the atomic matrix elements involved. Many of these matrix elements are similar to those required to calculate ionic polarizability, one of the few ion properties that can be independently measured at the level of precision required for the parity-violation studies. Precise polarizability measurements in Ba^+ can therefore provide valuable tests of the theoretical methods used to calculate the matrix elements required for the interpretation of the parity-violation experiments.

Another reason for particular interest in barium Rydberg fine-structure is the importance of nonadiabatic effects [3]. Because of the presence of a low-lying $5d$ level in Ba^+, the adiabatic expansion normally used to derive the long-range polarization model fails badly in barium. This behavior is expected to become more typical in studies of heavier Rydberg systems, where low-lying ionic excited states become more common. Studies in barium, where high-quality calculations of core properties exist, provide a good opportunity to perfect methods that accommodate nonadiabatic effects.

Several past studies have provided measurements of barium fine-structure intervals [3,4]. Other recent studies have discussed the surprising spin splittings observed in these studies [5,6]. Analysis of the observed fine-structure patterns has led to determinations of both dipole and quadrupole polarizabilities of the Ba^+ ion. The reported dipole polarizabilities are in very good agreement with theoretical calculations, but the inferred quadrupole polarizabilities have shown significant disagreement with calculations [4]. A similar disagreement in Si^{2+} has recently been shown to be due to neglect of higher-order terms in the analysis of the experimental data pattern [7]. We show here that the same explanation resolves the apparent disagreement over the quadrupole polarizability of Ba^+. When these higher-order terms are estimated and included in the analysis of the experimental data, good agreement with the calculated quadrupole polarizability is found. This study also extends the range of microwave fine-structure measurements to states of much higher L ($L \leq 11$) than studied previously, greatly strengthening the data pattern used for determining the polarizabilities.

II. EXPERIMENT

The RESIS microwave apparatus is shown schematically in Fig. 1. A beam of 9.5 keV Ba^+ ions, created in a Colutron ion source, undergoes single-electron capture in a Rb Rydberg target to form a beam of barium Rydberg states. The Rydberg target is formed from a thermal beam of Rb that is stepwise excited to its $9F$ state by three diode lasers [8]. The target density gives a charge capture probability of about 1%, giving a Rydberg population distribution centered around $n=9$ with a width of about 0.1 eV, so that approximately 10% of the capture is into $n=9$ Rydberg levels with all possible angular momentum states represented to some degree. Following the charge capture, all states with $n>15$ are Stark ionized in the preionizer and repelled out of the beam path. This is done in order to remove any initial upper Rydberg state population, which would be Stark ionized in the detector, causing a background regardless of laser excitation. Specific high-L Rydberg levels in the resulting fast beam can be excited upward by a Doppler-tuned CO_2 laser. The particular transitions observed in this study are the $n=9$ to the $n'=17$ and 20. An example of a typical optical line of such transitions was given in an earlier study [4]. In this work, higher precision is obtained by observing microwave-induced $\Delta n=0$ transitions in the upper state of the optical

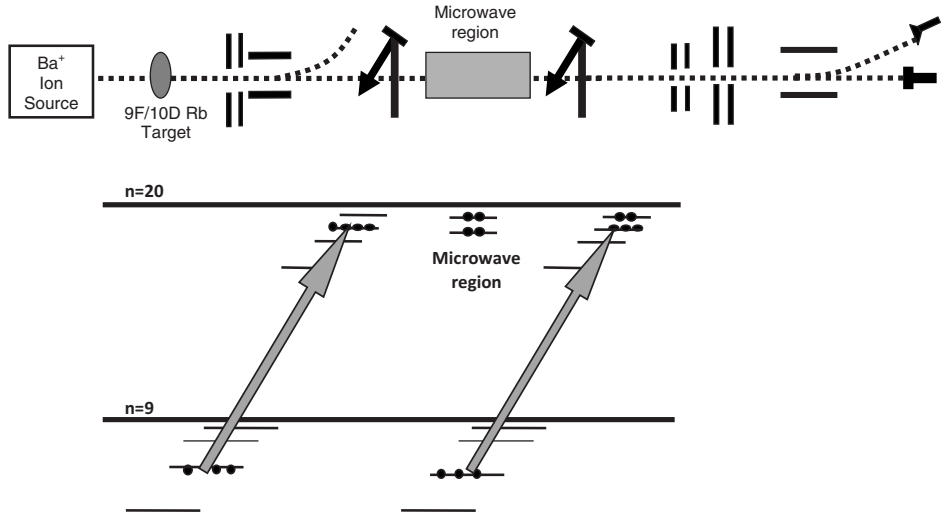

FIG. 1. Schematic diagram of microwave RESIS apparatus used for this study. An ion beam is created in a Colutron model-101 ion source. The ions are then collided with a selectively excited $9F$-$10D$ Rb target where some ions capture an electron. States of $n=15$ and higher are then Stark ionized in the preionizer and deflected with the remaining Ba^+ ions to be collected in a Faraday cup. Neutral barium atoms with $n<15$ enter the first CO_2 laser interaction region. Here a Doppler-tuned CO_2 laser excites a particular transition to a higher state of neutral barium, for example, $n=9$ atoms might be excited to $n=20$. The microwave region can then further excite a transition in the fine structure of the upper state, $n=20$, as described here. The second laser interaction region then repopulates the initial upper state if a microwave transition has occurred. The excited states are then Stark ionized in the stripper and focused by the lens, and the resulting signal ions are detected and collected on a channeltron plate while the neutral beam continues straight and is collected in a Faraday cup. Below the schematic, the fine structure of the $n=9$ and magnified $n=20$ high-L levels is illustrated. Each circle represents 1000 atoms residing in the energy level it is overlapping. The first laser puts population in both the $n=9$, $L=7$ and $n=20$, $L=8$ levels. A microwave transition moves 2000 of the $n=20$, $L=8$ atoms to the $n=20$, $L=9$ level. The second laser reequilibrates the $n=9$, $L=7$ and $n=20$, $L=8$ levels, putting an additional 1000 atoms in the $n=20$, $L=8$ state. All of the $n=20$ population will be ionized and detected. A total signal of 5000 ions is found if the microwave transition occurs, but only 4000 ions are detected if not.

transition. This is the same method used in earlier studies of H_2 Rydberg fine structure [9]. All angular momentum states of the upper Rydberg states will be ionized in the detector. In order to determine whether the angular momentum state has changed as a result of the microwave interaction, a second laser interaction region is inserted before the detector. Both CO_2 lasers are set to the same frequency and intersection angle with the atomic beam. The first laser populates a high-L state in an upper principal quantum state n. The second laser is used to repopulate the upper state if population has been transferred to a different angular momentum state by the microwave interaction. The detector consists of a Stark ionization region followed by a lens in order to refocus the charged signal beam. The deflection plates bend the path of the signal beam onto the channel electron multiplier. The combination of the two laser interaction regions and the microwave region creates a larger number of Stark ionized states detected when a microwave transition occurs. Most of the measured intervals were determined using electric-dipole-allowed $\Delta L=1$ transitions, but because of the limited resolution of the optical excitations it was necessary to determine the positions of the highest L levels using two-photon $\Delta L=2$ transitions.

The microwave interaction region is an eccentric coaxial transmission line excited by a traveling wave that propagates either parallel or antiparallel to the Rydberg beam. A HP microwave frequency generator produces the microwave field, which is amplitude modulated at 300 Hz. An example of a typical microwave resonance line shape is given in Fig. 2. The transit time T of the beam through the interaction region determines the linewidth $1/T$ of the transition. Two interaction regions were used in this study with slightly different geometries. One region of length 30 cm, which corresponds to a 0.7 MHz linewidth at 9.5 keV, has a maximum frequency limit of 2.4 GHz. The other region of length 20 cm with 1.05 MHz corresponding linewidth can reach frequencies of 6 GHz without excessive reflections. The microwave regions were shielded from motional fields due to the earth's magnetic field by two layers of μ metal.

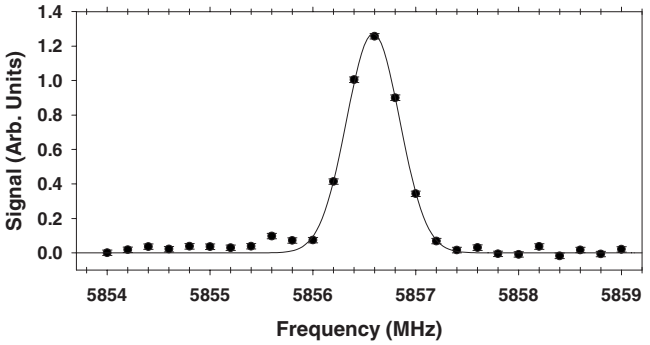

FIG. 2. Measured ionization current, using RESIS microwave techniques, plotted versus frequency, shows the barium copropagating $17I_{5.5}$–$17K_{6.5}$ transition in the 20 cm microwave region.

TABLE I. The Doppler-corrected measurements of $n=17$ and 20 barium transitions are listed, with the number of observations and the corresponding center of gravity between states of adjacent L. The two-photon interval measurements are indicated by an asterisk.

L, K-L', K'	No. of observations	ΔE_{obs} (MHz)	L-L'	$\Delta E_{c.g.}$ (MHz)
$n=17$				
6, 11/2-7, 13/2	3	5854.378(55)		
6, 13/2-7, 15/2	2	5633.388(28)	6-7	5735.175(41)
7, 13/2-8, 15/2	3	2439.890(62)		
7, 15/2-8, 17/2	3	2411.258(12)	7-8	2424.572(35)
8, 15/2-9, 17/2	2	1165.876(28)		
8, 17/2-9, 19/2	5	1157.800(45)	8-9	1161.588(37)
*8, 15/2-10, 19/2	3	885.064(31)		
*8, 17/2-10, 21/2	3	879.660(18)	9-10	602.811(63)
6, 13/2-7, 13/2	4	5592.712(85)		
$n=20$				
7, 13/2-8, 15/2	3	1518.669(47)		
7, 15/2-8, 17/2	6	1499.963(44)	7-8	1508.662(32)
8, 15/2-9, 17/2	3	727.808(75)		
8, 17/2-9, 19/2	4	722.431(87)	8-9	724.954(57)
9, 17/2-10, 19/2	2	378.323(28)		
9, 19/2-10, 21/2	2	376.556(40)	9-10	377.391(24)
*9, 17/2-11, 21/2	2	293.892(14)		
*9,19/2-11, 23/2	2	292.633(12)	10-11	209.068(31)
7, 15/2-8, 15/2	3	1492.124(30)		

A small ac Stark shift correction is applied to the line centers of the two-photon intervals, indicated by an asterisk in the tables. The power necessary for these transitions is significantly larger than for the single-photon transitions and as a result shifts due to the ac electric field driving the transitions are significant. Since the power necessary to saturate the transitions is different for each region because of the different geometry, the ac Stark shift must be calculated for each two-photon transition and each rf region. The ac Stark shifts for the barium $n=17$, $L=8-10$ interval were calculated to be 0.049(5) and 0.033(10) MHz for the 20 and 30 cm regions, respectively. Similarly, the $n=20$, $L=9-11$ interval has ac Stark shifts of 0.044(6) and 0.027(8) MHz. These calculated line shifts were applied as corrections to the two-photon line centers in Table I.

The line centers were determined by fitting the measured line shapes to a Gaussian, as illustrated for one case in Fig. 2. Measurements were taken with both orientations of microwave propagation, to average out first-order Doppler shifts. In some cases, measurements were taken with both physical orientations of the interaction region, to average out possible imbalance between the reflections from the termination region of the transmission line. The straight averages of the Doppler corrected line centers, for each of the 18 intervals measured in this study, are shown in Table I. The error bars are the larger of either the propagation of internal error or the external error from the scatter of the results. Two strongly allowed transitions with $\Delta K=\Delta L$ were observed between adjacent L levels, as a result of the significant spin splittings between the $K=L\pm 1/2$ Rydberg levels of common L. Figure 3 illustrates these transitions for a general case and also a possible weaker $\Delta K=0$ transition. For the case of the $n=17$, $L=6$ to $L'=7$ and $n=20$, $L=7$ to $L'=8$ transitions, this weaker $\Delta K=0$ transition was observed. These two $\Delta K=0$ transitions can be used in combination with the other $\Delta K=\Delta L$ transitions to establish the spin splittings δE_L in all of the levels studied. These derived spin splittings are shown in Table II. The frequency intervals between the centers of gravity of each L manifold can then be determined from the

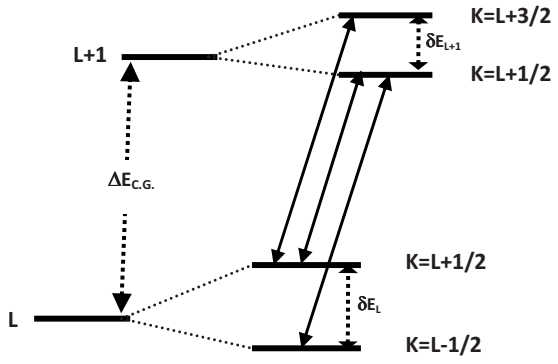

FIG. 3. Spin splitting for arbitrary L, with the solid arrows indicating the types of observed transitions, including the weaker $\Delta K=0$ transition. The dotted arrows label the energy between centers of gravity and the spin-splitting energies of the upper and lower levels.

TABLE II. Barium $n=17$ and 20 spin splittings δ_L, determined from observed RESIS microwave measurements.

$n=17$		$n=20$	
L	δE_L (MHz)	L	δE_L (MHz)
6	261.67(10)	7	26.545(56)
7	40.676(89)	8	7.839(53)
8	12.04(11)	9	2.46(13)
9	3.97(12)	10	0.70(14)
10	1.24(15)	11	−0.06(15)

two $\Delta K=\Delta L$ transitions, with a small correction depending on the spin splitting in the upper L level,

$$\Delta E_{\text{c.g.}} = \frac{(L+1)\Delta E_{K=L+1/2} + L\ \Delta E_{K=L-1/2}}{(2L+1)} - \frac{|\delta E_{L+1}|}{(2L+1)(2L+3)}. \tag{1}$$

Table I also shows the resulting determinations of the fine-structure intervals between centers of gravity of adjacent L levels in both $n=17$ and 20. The much smaller spin splittings due to the coupling of K to the Rydberg electron spin are unresolved here and ignored in the analysis.

III. ANALYSIS

The binding energy of a nonpenetrating Rydberg level differs only slightly from the hydrogenic value. The deviation is expressed in terms of an effective potential [7],

$$V_{\text{eff}}(r) = -\frac{C_4}{r^4} - \frac{C_6}{r^6} - \frac{C_7}{r^7} - C_{8L}\frac{L(L+1)}{r^8} - \frac{C_8}{r^8} + \cdots, \tag{2}$$

where each coefficient C_i is a property of the free ion core.

$$C_4 = \frac{\alpha_1}{2}, \quad C_6 = \frac{1}{2}(\alpha_2 - 6\beta_1),$$

$$C_7 = -\left(\frac{\delta}{2} + \frac{8}{5}\gamma\right) \quad C_{8L} = \frac{18}{5}\gamma, \tag{3}$$

and

$$\alpha_1 = \frac{2}{3}\sum_{n_c}\frac{|\langle gs||\vec{D}||n_c p\rangle|^2}{E(n_c p)}, \quad \alpha_2 = \frac{2}{5}\sum_{n_c}\frac{|\langle gs||\vec{\overleftrightarrow{Q}}||n_c d\rangle|^2}{E(n_c d)},$$

$$\beta_1 = \frac{1}{3}\sum_{n_c}\frac{|\langle gs||\vec{D}||n_c p\rangle|^2}{E(n_c p)^2}, \quad \gamma \cong \frac{1}{6}\sum_{n_c}\frac{|\langle gs||\vec{D}||n_C p\rangle|^2}{E(n_C p)^3},$$

$$\delta \cong \frac{4\sqrt{2}}{15}\sum_{n_C,n'_C}\frac{\langle g||\vec{D}||n_C p\rangle\langle n_C p||\vec{D}||n'_C d\rangle\langle n'_C d||\vec{\overleftrightarrow{Q}}||g\rangle}{E(n_C p)E(n'_C d)} + \frac{2\sqrt{30}}{45}\sum_{n_C,n'_C}\frac{\langle g||\vec{D}||n_C p\rangle\langle n_C p||\vec{\overleftrightarrow{Q}}||n'_C p\rangle\langle n'_C p||\vec{D}||g\rangle}{E(n_C p)E(n'_C p)}. \tag{4}$$

$\vec{D}$ and $\vec{\overleftrightarrow{Q}}$ represent the dipole and quadrupole moment operators acting on the $(N-1)$- electron core ion,

$$\vec{D} = \sum_{i=1}^{N-1} r_i C^{[1]}(\Omega_i), \quad \vec{\overleftrightarrow{Q}} = \sum_{i=1}^{N-1} r_i^2 C^{[2]}(\Omega_i). \tag{5}$$

$E(n_C P)$ and $E(n_C D)$ represent the excitation energies of the excited p and d states of the core ion and $C^{[\kappa]}(\Omega)$ denotes a spherical tensor of rank κ. The parameters α_1 and α_2 are the adiabatic dipole and quadrupole polarizabilities of the core ion, and β_1 is the first and γ the second in a sequence of "nonadiabatic" corrections to the dipole polarization energy [4,7]. The term proportional to the parameter δ represents the adiabatic dipole-dipole-quadrupole contribution to the perturbation energy [7]. The coefficient C_8 contains several higher-order parameters.

The energy of a particular Rydberg level is given in terms of V_{eff} by

$$E(n,L) = E^{[0]}(n) + E_{\text{rel}}(n,L) + \langle nL|V_{\text{eff}}|nL\rangle + \sum \frac{|\langle nL|V_{\text{eff}}|n'L'\rangle|^2}{[E^{[0]}(n) - E^{[0]}(n')]}, \tag{6}$$

where $E^{[0]}$ and E_{rel} are elementary hydrogenic expressions. Clearly, the first term in Eq. (6) does not contribute to the $\Delta n=0$ fine-structure intervals measured here. The third term provides the dominant contribution, but the second and fourth terms are not negligible. The second and fourth terms are referred to here as the relativistic and effective second-order energy contributions. In order to extract information about the coefficients in V_{eff} from experimental interval measurements, the small contributions of the relativistic and effective second-order energies are calculated and subtracted from the measured intervals to form quantities that may be regarded as direct expectation values of V_{eff}. These corrections and the resulting corrected intervals are shown in Table III. The contribution from the fourth term in Eq. (6), denoted $\Delta E^{[2]}$ in Table III, is estimated from only the leading term in V_{eff}, using the expression calculated by Drake and Swainson [10]. The uncertainty attached to this correction is an estimate of the possible error due to neglect of higher terms.

It has long been understood that the low-lying $5d$ state of Ba^+ introduces large nonadiabatic effects in the Rydberg fine structure. Actually the adiabatic expansion in the long-range model fails altogether for the quadrupole energy. This is due to the fact that the change in energy of the Rydberg state is not significantly smaller than that of the energy change of the ion core, and thus the expansion either does not converge or does so at a very slow rate. In order to accurately account for these nonadiabatic quadrupole effects, a multiplicative factor,

TABLE III. Summary of the corrections and scaling of the measured fine-structure intervals. The relativistic and effective second-order energy contributions are given in columns 3 and 4. Column 5 gives the calculated Stark shift rate κ of the observed transition. Also listed are the calculated expectation values of the radial matrix elements for the corresponding transitions and the normalized corrected energy. The intervals inferred from two-photon transitions are indicated by asterisks. Energies are given in MHz.

nL-$n'L'$	$\Delta E_{\text{c.g.}}$	ΔE_{rel}	$\Delta E^{[2]}$	κ [MHz/(V/cm)^2]	$\Delta\langle r^{-6}\rangle/\Delta\langle r^{-4}\rangle$	$\Delta\ E_{\text{corr}}/\Delta\langle r^{-4}\rangle$
17, 6-17, 7	5735.175(41)	0.732	102.158(293)	−5.5	0.00252	63.4506(38)
17, 7-17, 8	2424.572(35)	0.560	18.815(76)	−7.5	0.00136	62.0941(29)
17, 8-17, 9	1161.588(37)	0.442	4.252(29)	−10.3	0.00079	62.0289(35)
*17 9-17, 10	602.811(63)	0.358	1.123(14)	−12.7	0.00049	62.0414(79)
20, 7-20, 8	1508.662(32)	0.344	11.879(58)	−28.2	0.00141	62.1215(37)
20, 8-20, 9	724.954(57)	0.271	2.713(24)	−40.1	0.00083	62.0233(70)
20, 9-20, 10	377.391(24)	0.220	0.726(13)	−53.7	0.00052	61.9785(62)
*20 10-20, 11	209.068(31)	0.181	0.220(6)	−68.9	0.00034	61.9226(110)

called k_Q, is introduced. Gallagher *et al.* first presented this adjustment to the long-range model [3] and it was further modified by Snow *et al.* in an analysis of barium optical fine-structure data [4]. The correction factor allows for a separate treatment of the contribution due to this problematic $5d$ state, while the remaining contributions can be accurately modeled by the adiabatic expansion. This is achieved by defining k_Q as the ratio between the full contribution of the $5d$ state to the quadrupole polarization energy to that predicted in the adiabatic limit. The definition of k_Q is given explicitly in Eq. (A3) of Ref. [4], accounting for the $5d$ fine structure. The deviation from unity of this correction factor indicates the severity of the nonadiabatic effects. Table IV gives the values used in this work, k_Q-1, determined by use of the Dalgarno-Lewis technique. Notice the larger deviation from unity for the states of $L<7$.

TABLE IV. Calculated nonadiabatic multiplicative factors minus one, k_Q-1, used in this study. Values were calculated by the Dalgarno-Lewis method and include the fine-structure energies of the Ba^+ $5d$ states. The given values correspond to a weighted average of the values computed separately for the $K=L\pm1/2$ states. The results for the $L=5$ states were modified to account for a quantum defect of 0.05 in the $5d4f$ and $5d5f$ states.

(n,L)	k_Q-1	(n,L)	k_Q-1
(17,6)	0.614	(18,5)	−1.658
(17,7)	0.059	(19,5)	−1.612
(17,8)	−0.016	(20,5)	−1.573
(17,9)	−0.029	(21,5)	−1.540
(17,10)	−0.027	(18,6)	0.652
(20,7)	0.073	(19,6)	0.686
(20,8)	−0.011	(20,6)	0.718
(20,9)	−0.027	(21,6)	0.747
(20,10)	−0.026	(18,7)	0.065
(20,11)	−0.022	(19,7)	0.070
		(20,7)	0.073
		(21,7)	0.097

A final systematic correction is the possible Stark shift of the measured intervals due to a stray electric field in the microwave interaction region. Fortunately, the $n=17$ states of barium are much less affected by such a stray field than the $n=20$ transitions, as seen by the calculated shift rates listed in Table III. Consequently, we can use a comparison between fine-structure patterns observed in the $n=17$ and $n=20$ levels as a test for any such stray field. In order to account for stray electric fields, both sets of data can be consistently fitted to the leading terms of the polarization model and an additional term proportional to the contribution of Stark shifts to the pattern. The fit function is as follows:

$$\frac{\Delta E_{\text{corr}}}{\Delta\langle r^{-4}\rangle} = B_4 + B_6\left(\frac{\Delta\langle r^{-6}\rangle}{\Delta\langle r^{-4}\rangle}\right) + B_8\left(\frac{\Delta\langle r^{-8}\rangle}{\Delta\langle r^{-4}\rangle}\right) + B_0\left(\frac{\Delta[(k_Q-1)\langle r^{-6}\rangle]}{\Delta\langle r^{-4}\rangle}\right) + B_E\frac{\kappa}{\Delta\langle r^{-4}\rangle}, \quad (7)$$

where κ is the calculated Stark shift rate for each transition and B_E is the square of the stray electric field. The parameter B_0 is proportional to the contribution to the quadrupole polarizability from only the first excited core state, the Ba^+ $5d$ state.

A fit to the data pattern from Table I is unable to precisely determine all of the parameters in Eq. (7). Specifically, the data pattern is not strongly dependent on the nonadiabatic effects from the $5d$ state, so the curvature and therefore the initial slope are difficult to determine due to uncertainty in B_0. Fortunately, microwave data exist at lower-L states where the k_Q dependence is much stronger, and therefore these additional points allow a determination of the B_0 parameter and consequently reduce the uncertainty in the curvature and initial slope. The lower-L microwave data taken by Gallagher *et al.* include the $L=5$ to $L'=6$ and $L=6$ to $L'=7$ transitions of similar principal quantum state for $18\leq n\leq 21$ [3]. Snow *et al.* have shown that the grossly incongruent data can be fitted to a smooth curve when the dramatic effect of the low-lying $5d$ state is considered [4]. As in Ref. [4], the Gallagher *et al.* data are treated for the relativistic and effective second-order energy contributions. The error bars on the Gallagher *et al.*

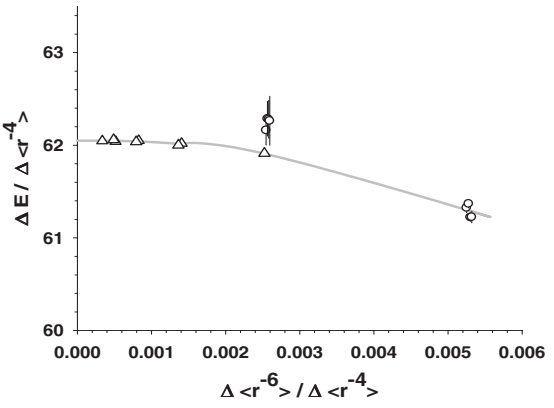

FIG. 4. Corrected intervals normalized to $\Delta\langle r^{-4}\rangle$ for both the microwave measurements of this study (triangles) and the $L=5$–6 and 6–7 measurements of Gallagher *et al.* [3]. (circles) are plotted here. The plotted values have been corrected for the effective second-order contributions, relativistic contributions, $5d$ nonadiabatic contributions, and Stark shifts as described in the text. The solid line represents the fit of Eq. (7) including only contributions from the first three terms.

data were expanded by a factor of 7 in order to make them internally consistent. This also allows for the uncertainty due to possible stray electric field Stark shifts.

The entire data pattern including these lower-L states is fitted to Eq. (7) with the following results:

$$B_4 = 62.049(15),$$

$$B_6 = 9(17),$$

$$B_0 = 762(4),$$

$$B_8 = -21\ 300(3100),$$

$$B_E = 0.0057(10).$$

The fit is excellent, and is illustrated by the plot shown in Fig. 4. Prior to plotting, the data are corrected for the relativistic, effective second-order, $5d$ nonadiabatic, and stray electric field contributions. Figure 4 plots these corrected fine-structure measurements normalized to $\Delta\langle r^{-4}\rangle$ versus $\langle r^{-6}\rangle/\langle r^{-4}\rangle$. The triangles indicate the data reported in this work, while the circles represent the previous microwave data of Gallagher *et al.* With the $5d$ nonadiabatic contribution removed, it can be seen that the data pattern does fit on a smooth curve predicted by the long-range model, shown here as a solid line.

The traditional interpretation of the parameters is as follows: the intercept B_4 is simply $C_4=\alpha_1/2$, and the slope B_6 is equal to $C_6=(\alpha_2-6\beta_1)/2$. In principle, B_0 gives one-half the $5d$ state contribution to the quadrupole polarizability, $B_0=\alpha_2^0/2$. The contribution of the higher-order terms proportional to $\Delta\langle r^{-7}\rangle/\Delta\langle r^{-4}\rangle$ and $\Delta[L(L+1)\langle r^{-8}\rangle]/\Delta\langle r^{-4}\rangle$, however, must first be assessed in order to determine if the above simple model is valid, as previously noted [7]. In order to assess the effect of the higher-order terms in the long-range polarization model, the contribution of these terms to the data pattern is evaluated. The smooth functions $\Delta\langle r^{-7}\rangle/\Delta\langle r^{-4}\rangle$ and $\Delta[L(L+1)\langle r^{-8}\rangle]/\Delta\langle r^{-4}\rangle$ versus $\Delta\langle r^{-6}\rangle/\Delta\langle r^{-4}\rangle$ can be very well parametrized by the following expression:

$$A_1 + A_2\left(\frac{\Delta\langle r^{-6}\rangle}{\Delta\langle r^{-4}\rangle}\right) + A_3\left(\frac{\Delta\langle r^{-8}\rangle}{\Delta\langle r^{-4}\rangle}\right). \tag{8}$$

Following the method of Snow and Lundeen [7], the values of $\Delta\langle r^{-7}\rangle/\Delta\langle r^{-4}\rangle$ and $\Delta[L(L+1)\langle r^{-8}\rangle]/\Delta\langle r^{-4}\rangle$ are calculated for each of the observed transitions and fitted to the function given in Eq. (8) with weights identical to those of the corresponding observed energy intervals. The parameters determined by the fit above indicate the magnitude at which the C_7 and C_{8L} terms contribute to the intercept and initial slope of this barium polarization plot. The fit to the $\Delta\langle r^{-7}\rangle/\Delta\langle r^{-4}\rangle$ points gives

$$A_1^{C7} = -1.07\times10^{-5},$$

$$A_2^{C7} = 0.0367,$$

$$A_3^{C7} = 6.56,$$

and the fit to $\Delta[L(L+1)\langle r^{-8}\rangle]/\Delta\langle r^{-4}\rangle$ finds

$$A_1^{C8L} = -1.92\times10^{-5},$$

$$A_2^{C8L} = 0.0641,$$

$$A_3^{C8L} = 20.87.$$

The fitted A_1 coefficients multiplied by the corresponding C_7 and C_{8L} parameters give the deviation of the fitted intercept in the polarization plot of these barium data, B_4, from the simple model of only C_4. The fits above give the following contribution to the intercept:

$$B_4 = C_4 - 1.07\times10^{-5}C_7 - 1.92\times10^{-5}C_{8L}.$$

Similarly, the slope of the polarization plot is found to be:

$$B_6 = C_6 + 0.0367C_7 + 0.0641C_{8L}.$$

Although the A coefficients are quite small, their contributions may still be significant depending on the magnitude of

TABLE V. Current and previous experimental values along with theoretical calculations of the polarizability of Ba^+ in atomic units [3,4,12].

	This work	Snow *et al.*	Gallagher *et al.*	Theory
α_1	123.88(5)	124.30(16)	125.5(10)	124.7(25)
α_2	4420(250)	2462(361)	2050(100)	4140

TABLE VI. Estimates of the contribution to the quadrupole polarizability of Ba^+ by the $5d$ state determined from current and previous experiments [5,3,6] are given along with the theoretical calculation in atomic units [12]. Agreement between experiment and theory is very poor, as discussed in the text.

	This work	Snow *et al.*	Gallagher *et al.*	Shuman and Gallagher	Theory
α_2^0	1524(8)	1828(88)	2050(100)	1562(93)	3318

C_7 and C_{8L}. These values can be estimated by including only the lowest excited core state in the calculation, under the assumption that this state is the largest contributor to the summation. Theoretical calculations of the matrix elements by relativistic all-order methods [11,12] with an assigned 1% uncertainty and experimental values for the energies give the following estimates:

$$C_7 = -2.99(6) \times 10^4,$$

$$C_{8L} = 1.11(2) \times 10^4.$$

These are merely estimated values, and it would be better to have complete calculations of both γ and δ from Eq. (4) to determine these coefficients. Using the fitted values of A_1 and A_2 along with the estimated coefficients above, the quantities of interest here, C_4 and C_6, are estimated to be

$$C_4 = B_4 - 0.320(6) + 0.213(4) = 61.942(25),$$

$$C_6 = B_6 + 1097(22) - 712(13) = 394(52).$$

Table V shows the dipole and quadrupole polarizabilities of Ba^+ obtained by use of the C_4 and C_6 values found above. For comparison, the previous experimental values [3,4] and the current theoretical calculations [12] are listed in Table V. The calculation of the quadrupole polarizability involves evaluation of β_1, the first nonadiabatic correction to the dipole polarizability. An accurate determination of β_1 can be obtained by applying a slight twist on the calculations performed by Curtis for the case of Kr^{6+} [13]. Use of precise experimental values of the $6P$ lifetimes and the dipole polarizability along with calculated branching fractions yields a value of $\beta_1 = 605(25)$ [14]. The experimental values found here of $\alpha_1 = 123.88(5)$ and $\alpha_2 = 4420(250)$ are completely consistent with the best theoretical calculations. Note the significant difference of a factor of 2 compared with the quadrupole polarizability reported in previous experiments, where higher-order contributions were neglected.

In theory, the B_0 parameter is a measure of the contribution of the $5d$ state to the adiabatic quadrupole polarizability of Ba^+ as discussed by Snow *et al.* [4],

$$\alpha_2^0 \equiv \frac{2}{5} \frac{|\langle 6s||\vec{\vec{Q}}||5d\rangle|^2}{E(5d)}. \tag{9}$$

The fitted value of B_0 would imply that $\alpha_2^0 = 1524(8)$, a value that is in very poor agreement with the calculated value, 3318 [12]. A separate analysis of barium spin-splitting data performed by Shuman and Gallagher [6] finds the reduced quadrupole matrix element of Ba^+ $\langle 6s||\vec{\vec{Q}}||5d\rangle = 9.76(29)$, which leads to a value of $\alpha_2^0 = 1562(93)$. Listed in Table VI are the determinations of α_2^0 for the current and previous experimental works and the theoretical calculation. The experimental values in the first three columns are all based on the nonadiabatic effects on the Rydberg fine-structure intervals, and therefore do not represent truly independent results. However, the analysis of Shuman and Gallagher, based on spin-splitting data, also gives a consistent result. The experimental results are in very poor agreement with the theoretical calculation, in contrast to the excellent agreement for the total dipole and quadrupole polarizabilities, shown in Table V. If the experimental values of α_2^0 are correct, the 6% agreement for the total quadrupole polarizability can only be a coincidence, since 80% of the calculated total quadrupole polarizability comes from the $5d$ level. On the other hand, it seems equally possible that the interpretations of both the B_0 parameter and the spin-splitting data are incomplete. Thus, in spite of the clear importance of the B_0 term in regularizing the L dependence of the fine-structure intervals, it is not yet clear whether the interpretation of the B_0 coefficient as a determination of α_2^0 is reliable.

IV. CONCLUSION

This study has greatly expanded the range of measured barium fine-structure intervals and increased their precision. Analysis of the measurements with the long-range polarization model has resulted in improved determinations of both dipole and quadrupole polarizabilities of the Ba^+ ion. In the case of the quadrupole polarizability, this determination resolves a factor of 2 discrepancy between theoretical calculations and earlier experimental reports. Large nonadiabatic effects were successfully treated using state-dependent correction factors k_Q. This procedure brings the $L=5$-6 and $L=6$-7 intervals, where nonadiabatic effects are large, into close agreement with higher-L intervals where nonadiabatic effects are small. Unfortunately, the scale of the nonadiabatic corrections does not seem to give a reliable determination of the $5d$ state's contribution to the quadrupole polarizability.

[1] S. R. Lundeen, Adv. At., Mol., Opt. Phys. **52**, 161 (2005).
[2] T. W. Koerber, M. Schacht, W. Nagourney, and E. N. Fortson, J. Phys. B **36**, 637 (2003).
[3] T. F. Gallagher, R. Kachru, and N. H. Tran, Phys. Rev. A **26**, 2611 (1982).
[4] E. L. Snow, M. A. Gearba, R. A. Komara, S. R. Lundeen, and W. G. Sturrus, Phys. Rev. A **71**, 022510 (2005).
[5] E. L. Snow, R. A. Komara, M. A. Gearba, and S. R. Lundeen, Phys. Rev. A **68**, 022510 (2003).
[6] E. S. Shuman and T. F. Gallagher, Phys. Rev. A **74**, 022502 (2006).
[7] E. L. Snow and S. R. Lundeen, Phys. Rev. A **75**, 062512 (2007).
[8] F. J. Deck, E. A. Hessels, and S. R. Lundeen, Phys. Rev. A **48**, 4400 (1993).
[9] W. G. Sturrus, E. A. Hessels, P. W. Arcuni, and S. R. Lundeen, Phys. Rev. A **44**, 3032 (1991).
[10] G. W. F. Drake and R. A. Swainson, Phys. Rev. A **44**, 5448 (1991).
[11] M. S. Safronova, W. R. Johnson, and A. Derevianko, Phys. Rev. A **60**, 4476 (1999).
[12] M. Safronova (private communication).
[13] L. J. Curtis, J. Phys. B **40**, 3173 (2007).
[14] Lorenzo J. Curtis (private communication).